Li, X., Li, Z-X., & Crewe, A. (2018). Nonlinear seismic analysis of a high-pier, long-span, continuous RC frame bridge under spatially variable ground motions. *Soil Dynamics and Earthquake Engineering*, *114*, 298-312. https://doi.org/10.1016/j.soildyn.2018.07.032

Nonlinear seismic analysis of a high-pier, long-span, continuous RC frame bridge under spatially variable ground motions

Xiaoqiong Li [a], Zhong-Xian Li [b,*], Adam J Crewe [c]

[a] *Key Laboratory of Coast Civil Structure Safety of Ministry of Education , Tianjin University, Tianjin 300350, China. lixiaoqiong@tju.edu.cn*
[b] *Key Laboratory of Coast Civil Structure Safety of Ministry of Education, Tianjin University, Tianjin 300350, China. zxli@tju.edu.cn*
[c] *Department of Civil Engineering, University of Bristol, Queens Building, University Walk, Bristol BS8 1TR, UK. a.j.crewe@bristol.ac.uk*

Highlights:

- A simulation method for SVGM with consideration of local site effects is developed.
- Both geometric and material nonlinear are considered in seismic analysis of the bridge.
- Uniform excitation is an alternative for seismic design of bridges on simple terrain.
- Multi-support excitation is necessary for large bridges on irregular terrain.
- The seismic design methods and codes for large bridges should be modified by applied SVGM.

Corresponding author at: School of Civil Engineering, Tianjin University, Tianjin 300350, China. Tel.: +86 22 23085888; fax: +86 22 23085555.
E-mail address: zxli@tju.edu.cn (Z.-X. Li).

Nonlinear seismic analysis of a high-pier, long-span, continuous RC frame bridge under spatially variable ground motions

Xiaoqiong Li [a], Zhong-Xian Li [b,*], Adam J Crewe [c]

[a] *Key Laboratory of Coast Civil Structure Safety of Ministry of Education, Tianjin University, Tianjin 300072, China.*
lixiaoqiong@tju.edu.cn

[b] *Key Laboratory of Coast Civil Structure Safety of Ministry of Education, Tianjin University, Tianjin 300072, China.*
zxli@tju.edu.cn

[c] *Department of Civil Engineering, University of Bristol, Queens Building, University Walk, Bristol BS8 1TR, UK.*
a.j.crewe@bristol.ac.uk

Abstract: Many very large bridges with high piers and long spans are under rapid construction in mountainous regions especially in Western China. However, the current seismic design methods in China are based on a code which only applies to bridges with span up to 150 m. To evaluate the risk of the inapplicable design method and the influence of spatially variable ground motions (SVGM) on the seismic response of very large bridges, a high-pier, long-span, continuous RC frame bridge is numerically studied. This study considers whether multiple support excitation can be simplified into specific uniform excitation cases while guaranteeing the conservative seismic demands for this bridge. Non-stationary SVGM on both bedrock and the surface of multiple soil layers are simulated including wave passage effects, coherency effects and site amplification effects. The nonlinear dynamic finite element model of the bridge is analysed for two groups of earthquake motions, namely group 1 - bedrock and group 2 - ground surface excitations. Each group contains three different excitations, i.e. i) multiple support excitation ii) the largest and iii) the smallest accelerations from the SVGM. The relative displacements, internal force responses and ultimate damage modes are obtained and compared. For this bridge the uniform ground motion input with the largest accelerations provides conservative seismic demands for most structural components when the site amplification effect is not considered (group 1). However, for the ground surface motions, where site amplification needs to be taken into account (group

Corresponding author at: School of Civil Engineering, Tianjin University, Tianjin 300072, China. Tel.: +86 22 23085888; fax: +86 22 23085555.
E-mail address: zxli@tju.edu.cn (ZX Li).

2), in several cases the uniform ground motion with the largest accelerations results in lower response than that predicted when considering SVGM. The present results indicate that only when the bridges are located on ideal simple topography where site effects have little influence, the uniform excitation with the largest accelerations taken from the SVGM may be an alternative input for seismic analysis. However, for bridges on complex terrain, where site effects can significantly amplify the ground motions at the bedrock, SVGM need to be applied as input for the seismic analysis. As spatial variability of input motion is not a mandatory requirement in the Chinese bridges design code, these results suggest that the existing design code for very large bridges should be modified accordingly.

Keywords: Spatially variable ground motions (SVGM); High-pier and long-span bridges; Seismic response; Nonlinear analysis; Multiple support excitation

1. Introduction

Recently many high-pier, long-span, continuous RC frame bridges have been constructed in mountainous regions, especially in Western China. These bridges are able to overcome the difficulties of providing transport facilities through deep valleys, and their high structural integrity can help to prevent catastrophic failure [1]. The Hezhang Bridge has piers up to 195 m high and the Beipanjiang Bridge has spans up to 290 m long, and more high-pier, long-span, continuous RC frame bridges are likely to be constructed in these mountainous regions [2].

Earthquakes occurring in mountainous regions can lead to catastrophic consequences. For example, many high-pier long-span bridges, serving as vital traffic arteries, were seriously damaged during the Wenchuan Earthquake on May 12, 2008. This not only significantly impeded the fast response of earthquake relief, but also resulted in long-term impacts to the regional traffic due to the difficulty of repair. A proper design should be able to enhance the resistance of bridge structures to seismic actions and reduce the damage effects. Unfortunately, understanding of the seismic behaviour of such large bridges is markedly insufficient. These high-pier, long-span continuous RC frame bridges in mountainous regions usually have box girder superstructures and thin-walled hollow piers with more than two fixed joints between the main piers and the girder [1-5]. This results in a more complex seismic

performance compared to normal road bridges. In particular, the piers of these large bridges usually have high flexibility to dissipate earthquake energy while the girders are designed to be more rigid in order to avoid excessive vertical deflections due to gravity. Moreover, high-pier, long-span continuous RC frame bridges often have asymmetric configurations to adapt to the irregular topography, resulting in different dynamic responses and failure modes compared to traditional symmetric beam bridges. Current practices of designing this type of bridges have to be based on guidelines or codes that only cover bridges up to a limited size and limited range of site parameters. For example, the China guideline for the seismic design of highway bridges [6] only applies to bridges with spans up to 150 m. No design principles or provisions for high-pier, long-span bridges are available yet.

In addition, during an earthquake event these long-span structures can also experience different ground motion excitations at each support point [7], which is known as spatially variable ground motions (SVGM) including wave passage effects, coherency effects and local site effects. Previous studies [1-5, 8-9] of large continuous RC frame bridges have indicated that the structural configuration and the spectral characteristics of the input motions have significant influence on the seismic response. There might be potential risks in using an inapplicable design code and ignoring the influence of SVGM when calculating the seismic response of large bridges in mountainous regions. Multi-support excitation is, unfortunately, beyond the scope of existing seismic design codes [10], expect Eurocode 8 that requires to consider the effects of SVGM when soil properties along a continuous bridge vary or the length of the continuous girder exceeds an appropriate limiting length [11]. SVGM are usually simulated through theoretical or semi-empirical power spectral density functions and coherency functions [12, 13]. However, most of these models can only roughly reflect the influence of local site effect. For valley topography with varying site conditions, Safak [14] obtained the vertical transfer function of shear waves in a horizontal medium layer based on the theory of seismic wave propagation. By applying the transfer function to the original spectral representation method, the spatially correlated ground motions can then be generated taking into account multiple soil layers and all site conditions.

Extensive numerical [1, 3-5, 10, 15-19] and experimental [20-23] studies have been conducted on the influence of multiple support excitation on bridges. A parametric analysis on the sensitivity of bridge response to SVGM conducted by Sextos et al. [24] indicates that the dynamic behaviour of bridges

subjected to SVGM cannot be adequately reproduced by uniform excitations, and site effects are an important part of the dynamic analysis process. However, like most previous studies, the pier height of the bridges studied only ranges from 4 m to 24 m, and the earthquake excitation is only applied in the transverse direction. Insufficient studies on the seismic performance of high-pier, long-span, continuous RC frame bridges under SVGM can be found in the literature. Therefore it is essential to carry out detailed seismic analysis to evaluate the different structural responses using uniform or SVGM for proper design of high-pier, long-span, continuous RC frame bridges. To accomplish this task, nonlinear dynamic analyses of an existing high-pier long-span continuous RC frame bridge are conducted in the present study. Both uniform and SVGM are taken into consideration in the numerical simulations. In particular, non-stationary SVGM on both bedrock and the surface of multiple soil layers are simulated including wave passage, coherency and site amplification effects. The structural responses including relative displacements, internal forces and damage modes of structural elements under different excitations are compared. Based on the results and analysis, suggestions are proposed to give direct solution for seismic design and facilitate the rapid construction of the high-pier, long-span continuous RC frame bridges in mountainous regions.

2. Construction details of the prototype

The high-pier, long-span continuous RC frame bridge selected in this study is Longtanhe Bridge located in Hubei, China [25]. Until recently it was one of the largest high-pier, long-span continuous RC frame bridges, but there are now dozens of new continuous RC frame bridges larger than this, with many more being built in mountainous regions especially in western China [2]. The seismic analyses presented in this paper will be particularly significant and relevant when considering the seismic capacity of these larger bridges.

Longtanhe Bridge is situated on varying site conditions as shown in Fig. 1, and has five spans (1@106 m, 3@200 m and 1@106 m, respectively). All piers of the bridge are cast by C50 concrete. The two high piers, namely Pier 2 and Pier 3, comprise double columns (with a spacing of 9 metres) connected by two tie beams. The columns have variable hollow rectangular cross sections, with a slope of 100:1 in longitudinal direction, and slopes of 100:1, 60:1 and 40:1 from top to bottom in transverse direction. The configurations of the column cross section are presented in details in Fig. 1. There are two HRB335

reinforcement layers in the piers, i.e., 20 mm diameter deformed bars at 150 mm spacing are embedded in the inside layer, and 32 mm diameter deformed bars at 150 mm spacing are embedded in the outside layer. By embedding Grade 270 low-relaxation pre-stressing strands within the C50 box girder, tri-axial tension control stress of 1395 MPa is applied. More details about this bridge can be found in [25].

Spatial variability of input motion is not a mandatory requirement in the Chinese bridges design code, and it is usually simplified into multiple support excitation without considering site amplification effects. However as aforementioned, site conditions may have significant influence on the seismic response of bridges. Thus SVGM on both bedrock and ground motions are applied to the seismic analyses in this study to investigate the necessity of considering SVGM.

3. Spatially variable ground motions (SVGM)

3.1 SVGM on bedrock

Ground motions at different locations on bedrock can be assumed to be a zero mean stationary stochastic process with the same power spectral density and simulated using the Clough-Penzien model [26]:

$$S_g(\omega) = \left|H_{\mathrm{g}}(\omega)\right|^2 \left|H_{\mathrm{f}}(\omega)\right|^2 S_0$$
$$H_{\mathrm{g}}(\omega) = \frac{{\omega_{\mathrm{g}}}^2 + 2\mathrm{i}\xi_{\mathrm{g}}\omega_{\mathrm{g}}\omega}{{\omega_{\mathrm{g}}}^2 - \omega^2 + 2\mathrm{i}\xi_{\mathrm{g}}\omega_{\mathrm{g}}\omega} \qquad H_{\mathrm{f}}(\omega) = \frac{\omega^2}{{\omega_{\mathrm{f}}}^2 - \omega^2 + 2\mathrm{i}\xi_{\mathrm{f}}\omega_{\mathrm{f}}\omega} \tag{1}$$

where S_0 is the constant power spectral density of white noise; $H_{\mathrm{g}}(\omega)$ is the Kanai-Tajimi filter function, with ω_{g} and ξ_{g} as the central frequency and damping ratio, respectively. $H_{\mathrm{f}}(\omega)$ is a high-pass filter applied to exaggerate the low-frequency component, with ω_{f} and ξ_{f} as the central frequency and damping ratio respectively.

The auto power spectral density function of each spatially correlated point in a one-dimensional earthquake field consisting n points on the ground surface and the cross power spectral density function between two arbitrary points can be presented as [27]:

$$S_{jj}(\omega) = \left|H_j(\mathrm{i}\omega)\right|^2 S_g(\omega)$$
$$S_{jk}(\mathrm{i}\omega) = H_j(\mathrm{i}\omega) H_k^*(\mathrm{i}\omega) S_g(\omega) \gamma_{j'k'}\left(d_{j'k'}, \mathrm{i}\omega\right) \qquad j,k = 1,2,...,n \tag{2}$$

where $H_j(\mathrm{i}\omega)$ and $H_k(\mathrm{i}\omega)$ are the site transfer function of two arbitrary points j and k on the ground surface, directly reflecting the influence of local site conditions on the wave propagation, and * means

complex conjugate. For the ground motions on bedrock $H_j(\mathrm{i}\omega)=H_k(\mathrm{i}\omega)=1$; $\gamma_{j'k'}(\mathrm{i}\omega)$ is the coherency function, showing the coherency effect of ground motions at point *j'* and point *k'*. Based on records from seismic arrays, several coherency function models have been proposed [8, 28].

The stationary stochastic time history of SVGM can be described using the $n\times n$ power spectral density matrix [7]:

$$\mathbf{S}(\mathrm{i}\omega)=\begin{bmatrix} S_{11}(\omega) & S_{12}(\mathrm{i}\omega) & \cdots & S_{1n}(\mathrm{i}\omega) \\ S_{21}(\mathrm{i}\omega) & S_{22}(\omega) & \cdots & S_{2n}(\mathrm{i}\omega) \\ \vdots & \vdots & \ddots & \vdots \\ S_{n1}(\mathrm{i}\omega) & S_{n2}(\mathrm{i}\omega) & \cdots & S_{nn}(\omega) \end{bmatrix} \tag{3}$$

where the diagonal elements $S_{jj}(\omega)\,(j=1,2,\ldots,n)$ are auto power spectral functions of frequency ω. The rest elements $S_{jk}(\mathrm{i}\omega)\,(j,k=1,2,\ldots,n,j\neq k)$ are complex cross-power spectral functions of frequency ω. The power spectral density matrix $\mathbf{S}(\mathrm{i}\omega)$ is a positive definite Hermite matrix and can be decomposed using the Cholesky factorization [8]:

$$\mathbf{S}(\mathrm{i}\omega)=\mathbf{L}(\mathrm{i}\omega)\left[\mathbf{L}^{*}(\mathrm{i}\omega)\right]^{\mathrm{T}} \tag{4}$$

where

$$\mathbf{L}(\omega)=\begin{bmatrix} L_{11}(\omega) & & & \\ L_{21}(\omega) & L_{22}(\omega) & & 0 \\ \vdots & \vdots & \ddots & \\ L_{n1}(\omega) & L_{n2}(\omega) & \cdots & L_{nn}(\omega) \end{bmatrix}_{n\times n} \tag{5}$$

The SVGM can be simplified into a one-dimensional stationary stochastic process $U(t)$ with multiple variables [29]:

$$U(t)=\left[u_1(t),u_2(t),u_3(t),\ldots,u_n(t)\right] \tag{6}$$

According to the original spectrum representation method [8], the earthquake acceleration time histories $u_j(t)\,(j=1,2,\ldots,n)$ at an arbitrary point could be expressed as:

$$u_j(t)=\sum_{k=1}^{j}\sum_{i=1}^{N}A_{jk}(\omega_i)\cos[\omega_i t+\theta_{jk}(\omega_i)+\varphi_{ki}(\omega_i)] \tag{7}$$

where $A_{jk}(\omega)=\sqrt{4\Delta\omega}\left|L_{jk}(\omega)\right|$ and $\theta_{jk}(\omega)=\tan^{-1}\left(\mathrm{Im}\left[L_{jk}(\omega)\right]\Big/\mathrm{Re}\left[L_{jk}(\omega)\right]\right)$ are the amplitude and phase of the generated acceleration time histories, whose frequency spectrum coincides with the target

spectrum in Eq. (2). N is the number of discretized frequency points; ω_{u} is the upper cut-off frequency, $\Delta\omega=\omega_{\mathrm{u}}/N$ is the frequency increment and $\omega_i=i\Delta\omega$. φ_i is the independent stochastic phase angle between 0 and 2π [30]. The stationary ground motion model is often multiplied by an envelope function $f(t)$ to achieve the non-stationary process [31]:

$$x_j(t)=f(t)\cdot u_j(t) \tag{8}$$

3.2 SVGM on the ground surface

The amplitude of earthquake ground motions can be significantly amplified when penetrating soft soil, which is known as the site amplification effect and can lead to crucial structural damage. However, research on the frequency spectrum of ground motion waves during the vertical propagation process through multiple soil layers is limited. Based on the theory of seismic wave propagation, Safak obtained the vertical transfer function of shear waves in horizontal medium layers [14]. For bedrock overlaid by a single soil layer, the relationship between the arbitrary point j on ground surface and the corresponding vertical projection point j' on bedrock can be expressed by a transfer function as:

$$H_j(\mathrm{i}\omega)=\frac{U_j(\mathrm{i}\omega)}{U_{j'}(\mathrm{i}\omega)}=\frac{(1+r_j-\mathrm{i}\xi_j)\mathrm{e}^{-\mathrm{i}\omega\tau_j(1-2\mathrm{i}\xi_j)}}{1+(r_j-\mathrm{i}\xi_j)\mathrm{e}^{-2\mathrm{i}\omega\tau_j(1-2\mathrm{i}\xi_j)}} \qquad (j=1,2,\ldots,n) \tag{9}$$

where $U_j(\mathrm{i}\omega)$ and $U_{j'}(\mathrm{i}\omega)$ are the Fourier transforms of the time histories $u_j(t)$ and $u_{j'}(t)$ at surface point j and bedrock point j', respectively. The damping ratio ξ_j denotes the attenuation effect caused by energy dissipation during the propagation process. $\tau_j=h_j/v_j$ is the propagation time of seismic waves from point j' to point j. r_j is the reflection coefficient of the upwards travelling waves within the soil layer, which is computed using Eq. (10):

$$r_j=\frac{\rho_r v_r-\rho_j v_j}{\rho_r v_r+\rho_j v_j} \tag{10}$$

This transfer function can be extended to a general function [14] for site conditions where bedrock is overlaid by m layers of soil ($m\geq 2$):

$$H_{Qm}(\mathrm{i}\omega)=\frac{\det\left|\mathbf{I}-\mathbf{\Lambda\Omega}_1\right|}{\det\left|\mathbf{I}-\mathbf{\Lambda\Omega}\right|}(1+r_m)q^{-\tau_m/T} \qquad q=\mathrm{e}^{\mathrm{i}\omega T} \tag{11}$$

where **I** is the $2m\times2m$ unit matrix; **Ω** is the $2m\times2m$ coefficient matrix, which is related to the reflection and penetration coefficient r of each soil layer. $\mathbf{\Omega}_1$ is the matrix obtained by replacing the column vector corresponding to u_1 with $(1, 0, 0, 0, \ldots, 0, 0, 0)^T$ in matrix **Ω**. **Λ** is the $2m\times2m$ diagonal matrix, in which the diagonal elements are comprised of the filtration coefficient λ caused by the damping of each soil layer, i.e., $\mathrm{diag}(\mathbf{\Lambda})=(\lambda_m, \lambda_m, \lambda_{m-1}, \lambda_{m-1},\ldots, \lambda_2, \lambda_2, \lambda_1, \lambda_1)$, and:

$$\lambda_i = \frac{1-\alpha_i}{2}\cdot\frac{1+q^{-1}}{1-\alpha q^{-1}} \qquad \alpha_i = \frac{1-\sqrt{1-\cos^2\theta_i}}{\cos\theta_i} \qquad \theta_i = \ln 2\cdot\frac{4\xi_i T}{\tau_i} \tag{12}$$

where T is the time interval; other variables are the same as previously mentioned.

Using the above parameters and equations and inputting the corresponding soil parameters, the transfer function $H_{Qm}(\mathrm{i}\omega)$ describing the filtration of a multi-layer soil can be solved. Finally, by substituting Eq. (9) or Eq. (11) into Eq. (2) and using the SVGM model proposed in section 3.1, the spatially variable ground motions with consideration of the local site effects can be obtained. More detailed validation is presented in [32].

4. Numerical modelling

4.1 Finite element model of the bridge

Most SVGM studies on high-pier long-span bridges employ partially linear models, especially for the superstructure, because the long spans usually lead to excessive deformations which makes the numerical analysis difficult with an inelastic nonlinear constitutive model. For this study a refined inelastic nonlinear finite element model of the whole bridge was created using ABAQUS. The constitutive and damage evolution properties of the C50 concrete adopted for the simulations are based on the code for design of concrete structures [33] as shown in Table 1 and Fig. 2. The two-scalar plastic-damage model for concrete proposed by Lee and Fenves [34] is adopted in this study. Two damage indices, namely D_t for tensile damage and D_c for compressive damage, ranging from 0 to 1, are independently introduced to account for different damage states, defined as:

$$\begin{aligned} &D_t = 1-\frac{\boldsymbol{\sigma}_t}{\bar{\boldsymbol{\sigma}}_t};\ D_c = 1-\frac{\boldsymbol{\sigma}_c}{\bar{\boldsymbol{\sigma}}_c} \\ &\bar{\boldsymbol{\sigma}}_t = \left(1-D_t\right)\mathbf{E}_0 : \left(\boldsymbol{\varepsilon}_t - \boldsymbol{\varepsilon}_t^{\,p}\right);\ \bar{\boldsymbol{\sigma}}_c = \left(1-D_c\right)\mathbf{E}_0 : \left(\boldsymbol{\varepsilon}_c - \boldsymbol{\varepsilon}_c^{\,p}\right) \end{aligned} \tag{13}$$

where $\boldsymbol{\sigma}_t$, $\boldsymbol{\varepsilon}_t$ and $\boldsymbol{\sigma}_c$, $\boldsymbol{\varepsilon}_c$ are stress and strain tensor of tension and compression, respectively. $\bar{\boldsymbol{\sigma}}_t$ and $\bar{\boldsymbol{\sigma}}_c$ are effective tensile and compressive stress; $\boldsymbol{\varepsilon}_t^p$ and $\boldsymbol{\varepsilon}_c^p$ are plastic part of tensile and compressive strain; $\mathbf{E}_0$ is initial elastic-stiffness tensor.

For computational efficiency and accuracy, S4R four-node shell elements are used to build the piers and main girder, and the mesh size is about 1 m × 1 m. The reinforcing layers are tied into the shell elements and B31 beam elements are included to simulate the stiff skeleton in the high piers as shown in Fig.1. An initial stress condition is introduced in the girder to apply the pre-stress. The finite element model of the whole bridge is shown in Fig. 3. Each end of the bridge is restrained in the transverse direction (*X*), vertical direction (*Z*), and *Y* rotation (*Ry*). The degree of freedom (DoF) at the connection points of piers and the main girders are coupled with the corresponding DoF of the girder, because they are fixed as a continuous frame bridge. Fixed boundary conditions are applied to the bottom of four piers. In this study the soil-structure interaction in different cases is assumed to be unchanged, thus the different seismic performance of the bridge subjected to SVGM and uniform ones can be easily determined. Through block-Lanczos method, the first eight natural frequencies and mode shapes of the bridge are shown in Fig. 4. Most modes have dominant transverse deflections owing to the lower stiffness in that direction, as this type of bridge usually does [1].

4.2 Earthquake ground motions at the site of bridge

The bridge is sited in a valley about 380 metres wide at the bottom and steep slopes on both sides. The soil layers are shown in Fig. 1, and the corresponding characteristic parameters are shown in Table 2 [6, 25]. The four points (No.1 to No.4) in Fig. 1 on the ground surface correspond to four pier support positions. According to JTG/T B02-01-2008 [6], the parameters in Eq. (1) for the horizontal earthquake ground motion on bedrock are:

$$\omega_g = 10\pi \text{ rad/s},\ \xi_g = 0.6,\ \omega_f = 0.5\pi \text{ rad/s},\ \xi_f = 0.6,\ S_0 = 0.0034\,\text{m}^2/\text{s}^2 \qquad (14)$$

which correspond to an earthquake with a time duration of 20 s (PGA = 0.2*g*, PGD = 0.082 m) [35].

Fig. 5 shows the filtered ground motion power spectral density function on the bedrock.

The coherency effect is calculated using the Sobczyk model [28]. For the ground motions of two arbitrary points *j*' and *k*' on bedrock, the coherency function can be expressed as:

$$\gamma_{j'k'}(\mathrm{i}\omega) = \left|\gamma_{j'k'}(\mathrm{i}\omega)\right| \mathrm{e}^{-\mathrm{i}\omega d_{j'k'}\cos\alpha/v_{\mathrm{app}}} = \mathrm{e}^{-\beta\omega d_{j'k'}^2/v_{\mathrm{app}}} \cdot \mathrm{e}^{-\mathrm{i}\omega d_{j'k'}\cos\alpha/v_{\mathrm{app}}} \quad (15)$$

where the coherency coefficient β is 0.0005, and $d_{j'k'}$ represents distance between any two support points. Assuming the angle α of the incident wave on the bedrock is 60°, the apparent velocity v_{app} can be taken as 1768 m/s based on the characteristics of the bedrock. It should be noted that the Sobczyk coherency model obtained from earthquake records on ground surface is used to model SVGM at bedrock, because no information about SVGM at the bedrock is available. And the same coherency model is used for the ground motions in three directions. The present assumption may lead to some inaccurate estimation of coherency loss. Further research into the influence of coherency function is deemed necessary. The upper cut-off frequency ω_{u} in the simulation process is assigned as 50π rad/s; the time duration T of the ground motion is 20 s and the time step dt is 0.01 s. Based on the aforementioned equations, a programme to calculate the SVGM was written, thus the triaxial ground motions at each support point of the bridge were obtained. For instance, the transverse (x axis) ground motion time histories at points 0' to 5' on the bedrock ignoring site effects, where the transfer function is $H_Q(\mathrm{i}\omega) = 1$, and those on the ground surface including site effects are shown in Fig. 6.

As shown in Fig. 6(a), the smallest and largest peak ground accelerations (PGAs) of the simulated earthquake time histories on bedrock are 1.85 m/s^2 (PGA of $x_{5'}$) and 2.56 m/s^2 (PGA of $x_{2'}$), respectively, which are close to the theoretical characteristics of the selected ground motion (PGA = 0.2g). On the ground surface (Fig. 6(b), the smallest and largest PGAs are 1.85 m/s^2 (PGA of x_5) and 4.46 m/s^2 (PGA of x_2), respectively, indicating the significant site amplification effect brought by the soil layers. The SVGM time histories in the y and z directions (not shown) were calculated using the same equations as those in the x direction. According to GB-50011-2010 code [33], the peak accelerations of triaxial ground motions were adjusted in the following ratio: 1 (x axis, transverse): 0.85 (y axis, longitudinal): 0.65 (z axis, vertical), reducing the PGAs for the y and z axis motions. This is because as shown in Fig. 4, the transverse direction (x) presents smaller stiffness. In addition to applying SVGM, two uniform excitation scenarios were also considered as alternative load cases. From the SVGM in Fig. 6, the triaxial motions with the largest x axis PGAs, generated at the support of Pier 2 (point 2) where the soil layers are relatively soft and complex, were considered as a uniform input for a 'Worst' case scenario,

because applying the largest PGA input at all supports might reasonably be assumed to cause the most severe damage to the bridge. Similarly, the ground motions with the smallest PGAs, generated at point 5, were used as uniform input for the 'Best' case scenario, where the smallest PGA is presumed to cause the lightest damage to the bridge. In total three input scenarios of triaxial ground motions on both bedrock (group 1) and the ground surface (group 2) are considered in this study, as shown in Table 3, taking the *x* direction as example.

5. Numerical results

The structural responses of the bridge under three excitations are numerically simulated. Significant differences between applied bedrock and ground surface motions can be observed by comparing the relative displacements, internal forces and ultimate damage modes of the bridge in different cases as detailed below.

5.1 Seismic analysis under ground motions on bedrock (group 1)

In this section, the ground motion accelerations shown in Fig. 6(a) at different supports with the smallest and largest SVGM PGAs are considered as the 'Best' case and 'Worst' case excitations respectively, as indicated in Table 3.

5.1.1 Relative displacements

Peak relative displacements at the top of Piers 1 to 4 under the three bedrock excitation scenarios are shown in Table 4. For all the excitation cases the piers have a larger response in the transverse (*x*) direction than that in the *y* and *z* directions. For the SVGM case, in particular, the peak displacement of Pier 3 in the *x* direction is more than 7 times that in the *y* direction, indicating that the transverse response of the bridge piers is a critical aspect of the seismic behaviour of this bridge.

Looking at the relative displacements presented in Table 4, the 'Worst' excitation case generally produces the highest displacement demand, as assumed. In the *x* direction, the 'Worst' case generates about a 30% larger relative displacement at the top of high piers than the other two excitation scenarios, although it is only 9% larger for the short piers. In the *y* direction, the relative displacement of the high piers under the 'Worst' case motion is approximately three times larger than the other two input motions, but the *y* displacements of Pier 1 under the three excitation scenarios are fairly similar. In the *z* direction, the vertical displacement of the high piers is about twice as much as that of the short piers, but there is

little difference between the relative displacement responses under the three excitation scenarios. These results show that the high piers are more responsive than the short piers due to their higher flexibility.

Fig. 7 presents the peak relative transverse (x) displacements for short Pier 1 and high Pier 3 as they represent the smallest and largest responses of all the piers. For Pier 3 (the high pier), the 'Worst' case excitation clearly produces the largest displacement demand while the 'Best' case creates the smallest demand at all points up the pier. However, for Pier 1 (the short pier), whilst the 'Worst' case excitation does produce a slightly larger response at the top of pier, the relative displacements in the other two cases are almost identical and overall, the relative displacement responses of Pier 1 are similar.

5.1.2 Internal forces

Fig. 8 shows the internal force demand envelopes of absolute axial force in the longitudinal (y) direction, shear force in the transverse (x) direction and bending moment about x axis of the bridge girder under three different excitation cases. The girder and pier locations are indicated at the bottom of each figure.

The 'Worst' excitation case creates the highest seismic force demands along most of the bridge girder. The peak axial forces occur at the joints between the girder and piers, as well as in the mid-spans. The data show particularly sharp increases at the joints, which are vulnerable points for this bridge under seismic excitation. This is because the joints between piers and girder are fixed in a continuous frame bridge, thus they usually suffer from large axial forces and subsequent localised damage. However, the peak shear forces occur at mid-spans also in accordance with the positions where peak relative displacements take place. The curve of bending moments shows similar fluctuation tendency with shear forces along the main girder, which are relatively larger at the mid-spans than those at other locations.

5.1.3 Damage analysis

The damage indices ranging from 0 to 1 derived from the numerical results can be used to describe the extent of seismic damage to the bridge [34]. The lower and upper bound indicate undamaged and completely damaged status, respectively. The damage modes for the three excitation cases are compared. Diagrams of the compressive and tensile damage distributions are shown in Fig. 9 and Fig. 10, respectively.

As can be seen, Fig. 9 shows that the plastic compressive damage is limited to relatively small areas of the bridge while in Fig. 10 it can be observed that the plastic tensile damage is much more widespread, especially on the bridge girder. In comparison, the plastic tensile damage in the piers is focused in the tie beams between the two columns of the high piers. The compressive and tensile damage development time history curves of the bottom tie beam on Pier 3 shown in Fig. 11 also indicate that, the tensile damage of the tie beam is much larger than compressive damage. The ultimate tensile damage index under three excitation scenarios (0.396 for SVGM, 0.698 for the 'Worst' cases, and 0.546 for the 'Best' case) is about 4 to 9 times of the ultimate compressive damage index (0.041, 0.169, and 0.077, respectively).

Compared with two uniform excitation cases (the 'Best' and 'Worst' cases), SVGM results in girder damage that tends to shift towards the direction to the shortest Pier 1 as shown in Figs. 9 and 10, which alleviates the right part of each span. Meanwhile, the tensile damage in the tie beams subjected to SVGM is reduced by about half in comparison with that subjected to the 'Worst' case excitation (Fig. 11).

Overall, the data and figures show that most components in this bridge have the largest seismic response when subjected to the 'Worst' case excitation. For this bridge, the uniform ground motion input with the largest PGA (the 'Worst' case) provides conservative seismic demands for most structural components when the site amplification effect is not considered (on bedrock), which suggests that the uniform excitation with the largest PGA taken from the spatially variable ground motions may be an alternative input for large bridges located on ideal simple topography where site effects have little influence.

5.2 Seismic analysis under ground motions on ground surface (group 2)

In this section, the ground motion accelerations which take the site amplification effects into account shown in Fig. 6(b) at different supports with the smallest and largest SVGM PGAs are considered as the 'Best' case and 'Worst' case excitations respectively, as indicated in Table 3.

5.2.1 Relative displacements

The peak relative displacements at the top of Pier 1 to Pier 4 under the three ground surface excitation scenarios are summarized in Table 5. Again, for all these excitation cases, the piers have the largest

responses in the transverse (x) direction. For the 'Worst' case excitation the peak displacement of Pier 3 in the x direction is more than 18 times larger than that in the y direction. Particularly for the high piers, the 'Best' case results in significantly smaller relative displacements at the tops of all the piers than those in the other two excitation scenarios. For example, the relative displacement generated on Pier 3 by the 'Best' case is only 28.7% of that by the 'Worst' case and 34.8% of SVGM cases; and the displacements of the piers subjected to 'Worst' case excitation are the largest among three excitation scenarios except for Pier 4. However, the data in Table 5 show that the 'Worst' case does not always produce the highest displacement demand, especially in the y direction. The relative displacements of Piers 2, 3 and 4 under SVGM are approximately 3 to 5 times larger than either the uniform cases. However, the displacements of Pier 1 under all three excitation scenarios are quite similar. Same observation can also be found in Section 5.1. In the z direction, the vertical displacement of the high piers is about twice that of short piers, and the 'Worst' case leads to the largest displacement response of all piers. Compared to the previous bedrock excitation cases, when the site amplification effect is taken into account, the SVGM can lead to some particularly large displacement responses, especially in the longitudinal (y) direction of bridge. These results show that for those bridges on complex terrain where site effects can significantly amplify the ground motion waves transferred from bedrock, SVGM need to be applied as inputs for any seismic analysis.

Fig. 12 shows the peak relative transverse (x) displacements for short Pier 1 and high Pier 3 as they represent the smallest and largest responses of all the piers. For both piers, the 'Worst' case excitation produces the largest displacement demand while the 'Best' case produces the smallest. However, for Pier 1 (the short pier) the displacements due to SVGM are more similar to the 'Best' case, whereas for Pier 3 the displacements due to SVGM are almost as bad as the 'Worst' case.

5.2.2 Internal forces

Fig. 13 shows the demand envelopes of absolute axial force in the longitudinal (y) direction, shear force in the transverse (x) direction and bending moment about x axis of the bridge girder subjected to three different excitation cases. By comparing Figs. 8 and 13, when site amplification effect is considered, SVGM creates as much seismic force demand throughout the length of the bridge as the

'Worst' case does. This is particularly noticeable at the locations where the peak axial forces and shear forces take place, which are concentrated at joints and mid-spans.

Sometimes the piers, especially high piers, are more vulnerable during earthquakes. Therefore, the absolute internal force demand envelope of Pier 2 is shown in Fig. 14. The shear force is transverse shear force in x direction, and the moment is bending moment force about y axis. Basically, along the entire pier, shear force demands for SVGM are higher than other scenarios. Especially Fig. 14(a) suggests a higher demand in shear forces at the bottom of Pier 2, which is not well captured by the identical motions. As shown in Fig. 14(b), it is quite obvious that the bending moments along the pier height are significantly amplified by 3 to 5 times at the connection points of the pier and tie beams, but slightly reduced at the clap boards. The SVGM produces a higher bending moment demand at the upper tie beam, while the Worst case generates a higher demand at the lower tie beam. Although tie beams are set to reduce the slenderness ratio of high piers and improve their stability, they result in moment concentration and become potential risks to the seismic performance of the bridge.

5.2.3 Damage analysis

The compressive damage and tensile damage distribution diagrams obtained from the numerical simulations are shown in Fig. 15 and Fig. 16, respectively. Overall, most damage is concentrated at the mid-spans and in the tie beams between two columns of the high piers, but these load cases also cause some tensile damage at the bottom of the short piers.

Similar to the observation in Section 5.1, the tensile damage is spread more widely throughout the bridge than the compressive damage. The compressive damage is mainly located at mid-spans, while the tensile damage in the girder is more widely distributed. However, the stress concentration at the ends of the tie beams is severe and high enough to cause fracture. Figs. 15 and 16 show that the tie beams obviously suffer much larger tensile damage than compressive damage. Therefore the tensile damage development time history curves of the upper and bottom tie beams on Pier 3 are shown in Fig. 17. It indicates that the uniform input motions result in much lower ultimate tensile damage index (0.283 for the 'Worst' case, and 0.136 for the 'Best' case) than that predicted by SVGM (0.708) for the upper tie beam. Under the 'Worst' uniform excitation, tensile damage on the upper tie beams seems to be relieved while that in the lower ones is aggravated, as compared with SVGM case. The high piers suffer

the most from the ground motions with large peak accelerations (SVGM and the 'Worst' case). As the piers display different failure modes when subjected to these two excitation cases, it is inadequate to consider the uniform excitation, even with the largest peak accelerations as a replacement for SVGM.

By comparing the tensile damage shown in Fig. 10 and Fig. 16, it can be observed that the ground surface motions are causing more damage in the tie beams but, more significantly, damage is now also occurring in the piers themselves. This is particularly obvious in the SVGM and 'Worst' cases. The very high damage indices in the tie beams suggest that they would suffer from fracture and subsequent failure. Then, without the support from the tie beams, the high piers could easily lose their stability, in spite of their high strength capacity and low damaged status, which would pose a threat to the whole bridge.

Comparison between Fig. 10 and Fig. 16 also indicates that site effects significantly amplify the nonlinear seismic response of this continuous RC frame bridge. For instance, tensile damage appears at the bottom of short piers when the site effect is considered, which vanishes in Fig. 10. These results show that site amplification effects cannot be ignored during seismic analysis, otherwise a significant underestimation of dynamic response and damage of the high-pier, long-span bridge can be resulted. Overall, for those bridges on complex terrain, where site effects can significantly amplify the ground motion waves transferred from bedrock, analysis including spatially variable ground motions is strongly recommended as an appropriate input for seismic design.

6. Conclusion

This study qualitatively evaluates whether multiple support excitation can be simplified into a uniform one to satisfy the conservative seismic demands for a very large continuous RC frame bridge in mountainous regions with complex soil conditions. The investigations were carried out by means of numerical simulations. Comparisons of the bridge responses under different excitations provide some specifications for seismic design and analysis of the high-pier, long-span, continuous RC frame bridges. For instance, the tie beams are potential risks to the seismic performance. When taking site effects into consideration, the peak relative transverse displacement at the top of the high pier might be more than doubled, and the ultimate tensile damage of the tie beam on high pier is increased by about 20%.

While additional research needs to be conducted for further quantification, the present study provides new insights that give significant contribution to the seismic design criteria specifically for high-pier, long-span, continuous RC frame bridges as summarized below:

When the site effect is not considered (on bedrock), the uniform ground motion input with the largest accelerations provides conservative seismic demands for the bridge, making it suitable as an alternative input for seismic analysis of high-pier, long-span, continuous RC frame bridges. However, this approach might result in underestimation of the bridge response when it comes to ground surface motions where site amplification has to be accounted. Accordingly, it is recommended to adopt spatially variable ground motions (SVGM) as the input for seismic analysis of such type of bridges on complex terrain where site effects can significantly amplify the ground motion waves transferred from bedrock. As SVGM is currently not a mandatory requirement in the Chinese bridges design code, usually it is simplified as travelling wave without site amplification. Thus based on the qualitative conclusion from this study, the current design code should be updated as soon as possible with additional considerations for high-pier, long-span, continuous RC frame bridges for compliance with the rapid construction in mountainous regions.

7. Acknowledgements

The authors gratefully acknowledge the financial supports for this research by the National Natural Science Foundation of China under grant number 51427901 and 91315301 and the National Basic Research Program (973 Program) of China under grant number 2011CB013603.

8. Reference

[1] Jia HY, Zhang DY, Zheng SX, Xie WC, Pandey MD. Local site effects on a high-pier railway bridge under tridirectional spatial excitations: Nonstationary stochastic analysis. Soil Dynamics and Earthquake Engineering 2013; 52: 55-69.

[2] Hu N, Dai GL, Yan B, Liu K. Recent development of design and construction of medium and long span high-speed railway bridges in China. Engineering Structures 2014; 74: 233-241.

[3] Zhou G, Li X, Qi X. Seismic response analysis of continuous rigid frame bridge considering canyon topography effects under incident SV waves. Earthquake Science 2010; 23(1): 53-61.

[4] Zhang DY, Jia HY, Zheng SX, Xie WC, Pandey MD. A highly efficient and accurate stochastic seismic analysis approach for structures under tridirectional nonstationary multiple excitations. Computers & Structures 2014; 145: 23-35.

[5] Liu X, Fan J, Nie J, Li G. Behavior of composite rigid frame bridge under bi-directional seismic excitations. Journal of Traffic and Transportation Engineering 2014; 1(1): 62-71.

[6] Guidelines for Seismic Design of Highway Bridges. JTG/T B02-01-2008. Beijing: China Communications Press, 2008.

[7] Zerva A, Zervas V. Spatial variation of seismic ground motions: an overview. Applied Mechanics Reviews 2002; 55(3): 271-297.

[8] Hao H, Oliveira CS, Penzien J. Multiple-station ground motion processing and simulation based on SMART-1 array data. Nuclear Engineering and Design 1989; 111(3): 293-310.

[9] Yoshikawa M, Hayashi H, Kawakita S, Hayashida M. Construction of Benten Viaduct, rigid-frame bridge with seismic isolators at the foot of piers. Cement and Concrete Composites 2000; 22(1): 39-46.

[10] Lou L, Zerva A. Effects of spatially variable ground motions on the seismic response of a skewed, multi-span, RC highway bridge. Soil Dynamics and Earthquake Engineering 2005; 25(7): 729-740.

[11] European Standard EN 1998-2: 2005. Eurocode 8: Design of structures for earthquake resistance, Part2: Bridges. Brussels: European Committee for Standardization, 2005.

[12] Deodatis G. Simulation of ergodic multivariate stochastic processes. Journal of Engineering Mechanics 1996; 122(8): 778-787.

[13] Kiureghian A. A coherency model for spatially varying ground motions. Earthquake Engineering & Structural Dynamics 1996; 25(1): 99-111.

[14] Şafak E. Discrete-time analysis of seismic site amplification. Journal of Engineering Mechanics 1995; 121(7): 801-809.

[15] Karmakar D, Ray-Chaudhuri S, Shinozuka M. Seismic response evaluation of retrofitted Vincent Thomas bridge under spatially variable ground motions. Soil Dynamics and Earthquake Engineering 2012; 42: 119-127.

[16] Chouw N, Hao H. Study of SSI and non-uniform ground motion effect on pounding between bridge girders. Soil Dynamics and Earthquake Engineering 2005; 25(7): 717-728.

[17] Mehanny SS, Ramadan OM, El Howary HA. Assessment of bridge vulnerability due to seismic excitations considering wave passage effects. Engineering Structures 2014; 70: 197-207.

[18] Wang J, Carr AJ, Cooke N, Moss PJ. The response of a 344 m long bridge to non-uniform earthquake ground motions. Engineering structures 2009; 31(11): 2554-2567.

[19] Sextos AG, Kappos AJ, Mergos P. Effect of soil-structure interaction and spatial variability of ground motion on irregular bridges: the case of the Krystallopigi bridge. In Proc., 13th World Conference on Earthquake Engineering Aug 1-6, Vancouver, Canada; 2004.

[20] Li B, Bi K, Chouw N, Butterworth JW, Hao H. Experimental investigation of spatially varying effect of ground motions on bridge pounding. Earthquake Engineering & Structural Dynamics 2012; 41(14): 1959-1976.

[21] Williams D, Godden W. Seismic response of long curved bridge structures: experimental model studies. Earthquake Engineering & Structural Dynamics 1979; 7(2): 107-128.

[22] Crewe AJ, Norman JA. Experimental modelling of multiple support excitation of long span bridges. In Proceedings of the 4th International Conference on Earthquake Engineering Oct 12-13, Taipei, Taiwan; 2006.

[23] Li X, Zhang DY, Yan WM, Chen YJ, Xie WC. Shake-table test for a typical curved bridge: Wave passage and local site effects. Journal of Bridge Engineering 2014; 20(2): 04014061.

[24] Sextos AG, Kappos AJ, Pitilakis KD. Inelastic dynamic analysis of RC bridges accounting for spatial variability of ground motion, site effects and soil–structure interaction phenomena. Part 2: Parametric study. Earthquake Engineering & Structural Dynamics 2003; 32(4): 629-652.

[25] Luo YK, Feng PC. Design of Longtanhe river bridge. Bridge Construction 2005; 2: 29-32.

[26] Clough RW, Penzien J. Dynamics of structures. New York: McGraw Hill, Inc. 1993.

[27] Hao H, Chouw N. Modeling of earthquake ground motion spatial variation on uneven sites with varying soil conditions. In the 9th International Symposium on Structural Engineering for Young Experts Aug 18-21, Fuzhou, China; 2006.

[28] Sobczky K. Stochastic wave propagation. Netherlands, Kluwer Academic Publishers. 1991.

[29] Di Paola M, Zingales M. Digital simulation of multivariate earthquake ground motions. Earthquake engineering & structural dynamics 2000; 29(7): 1011-1027.

[30] Shinozuka M. Monte Carlo solution of structural dynamics. Computers & Structures 1972; 2(5): 855-874.

[31] Rodolfo Saragoni G, Hart GC. Simulation of artificial earthquakes. Earthquake Engineering & Structural Dynamics 1973; 2(3): 249-267.

[32] Li ZX, Li XQ, Li N. Simulation of Multi-support and Multi-dimension Spatially Correlated Earthquake Ground Motions. Earthquake Engineering and Engineering Dynamics 2014; 34(4): 66-74.

[33] Code for design of concrete structures. GB-50010-2010. Beijing: China Architecture & Building Press, 2010

[34] Lee J, Fenves GL. Plastic-damage model for cyclic loading of concrete structures. Journal of engineering mechanics 1998; 124(8): 892-900.

[35] Bi K, Hao H. Numerical simulation of pounding damage to bridge structures under spatially varying ground motions. Engineering Structures 2013; 46: 62-76.

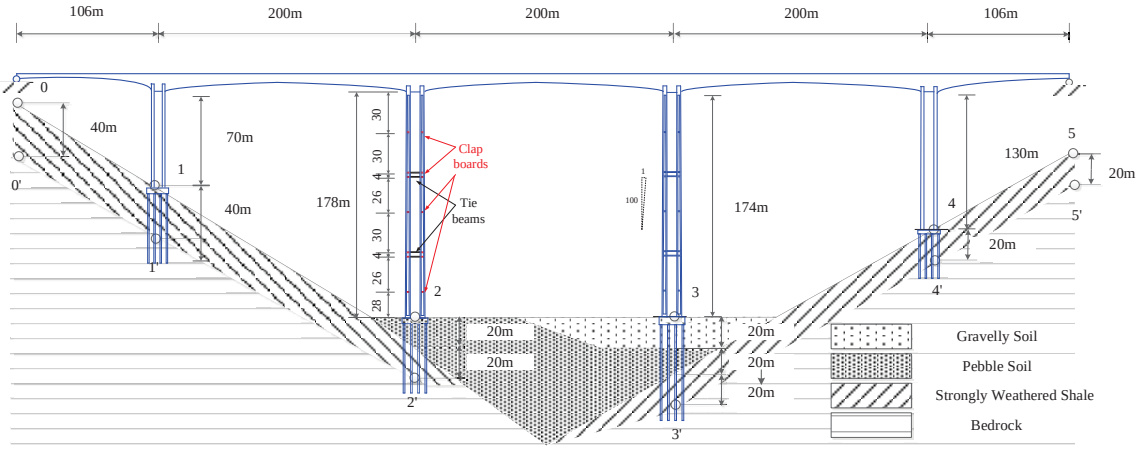

(a) Elevation view of the bridge

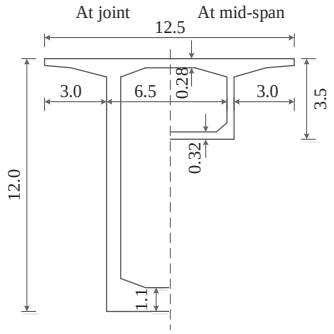

(b) Cross section of girder

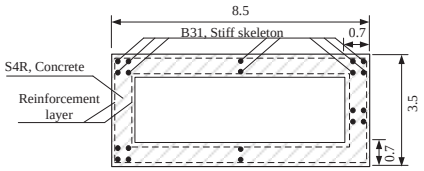

(c) Top section of pier columns

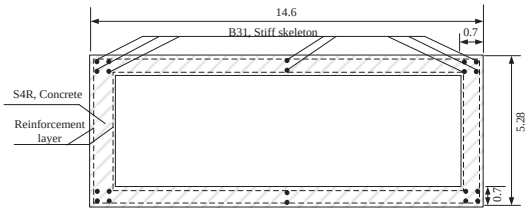

(d) Bottom section of Pier 2's columns

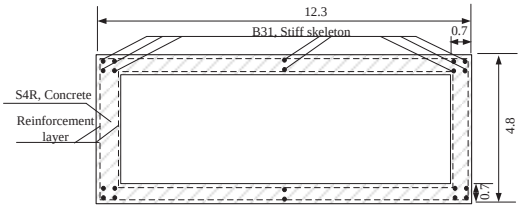

(e) Bottom section of Pier 4's columns

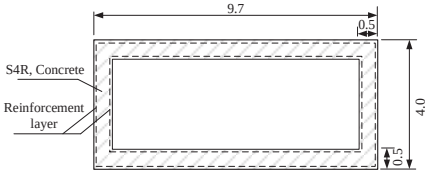

(f) Cross section of upper tie beams

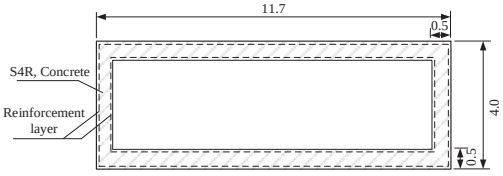

(g) Cross section of bottom tie beams

Fig. 1 Schematic view of the high-pier, long-span, continuous RC frame bridge (m)

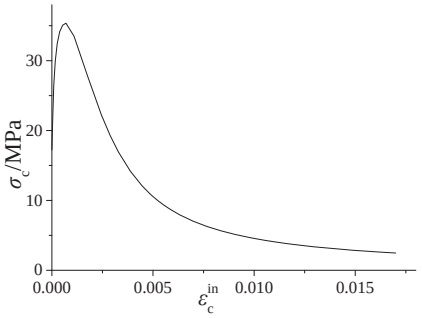

(a) σ_c-ε_c^{in} compressive stress-strain properties

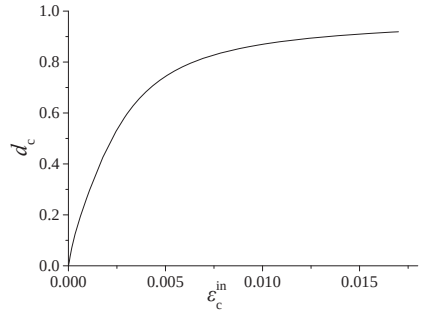

(b) d_c-ε_c^{in} compressive damage evolution

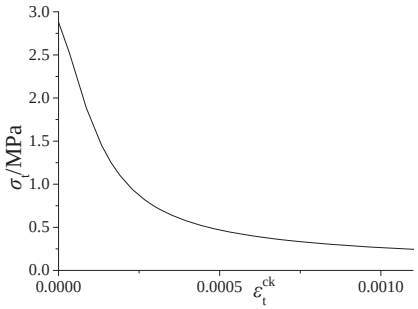

(c) σ_t-ε_t^{ck} tensile stress-strain properties

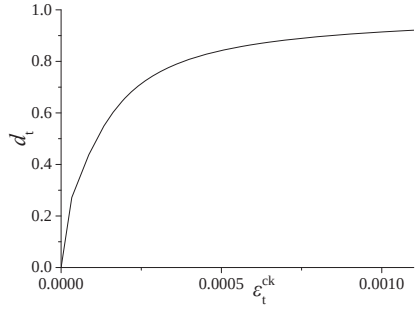

(d) d_t-ε_t^{ck} tensile damage evolution

Fig. 2 Damage constitutive relations for concrete C50

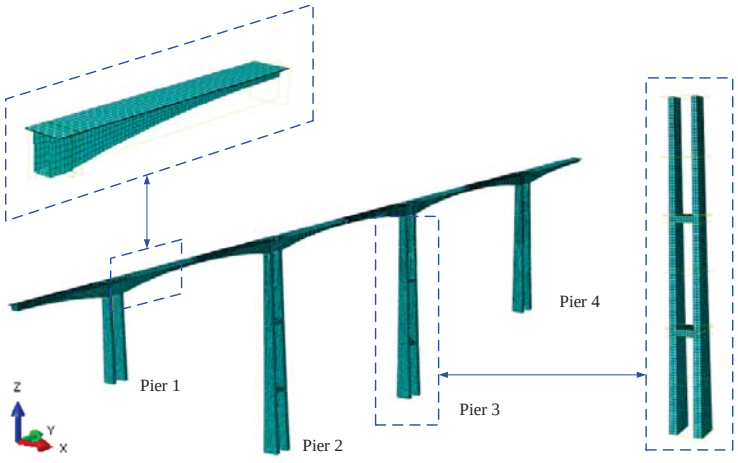

Fig. 3 Finite element model of the bridge

Mode 1 f_1=0.1751Hz
1st transverse mode

Mode 2 f_2=0.2360Hz
2nd transverse mode

Mode 3 f_3=0.3622Hz
3rd transverse mode

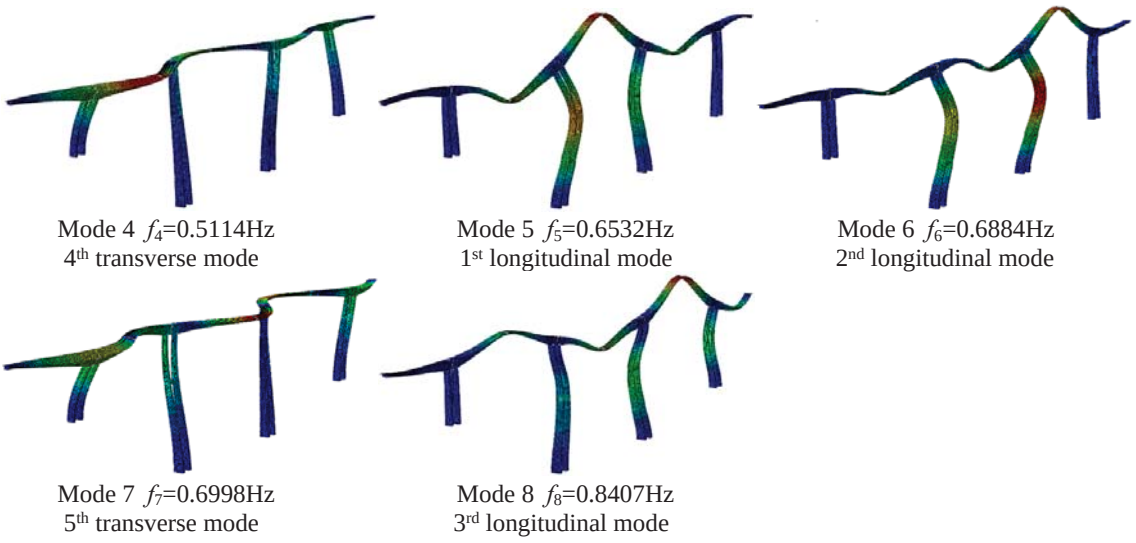

Fig. 4 Mode frequencies and shapes of the bridge (expanded scale)

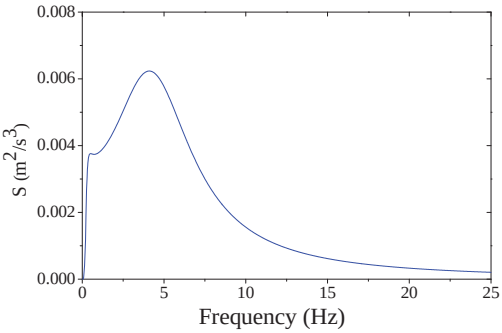

Fig. 5 Power spectral density function

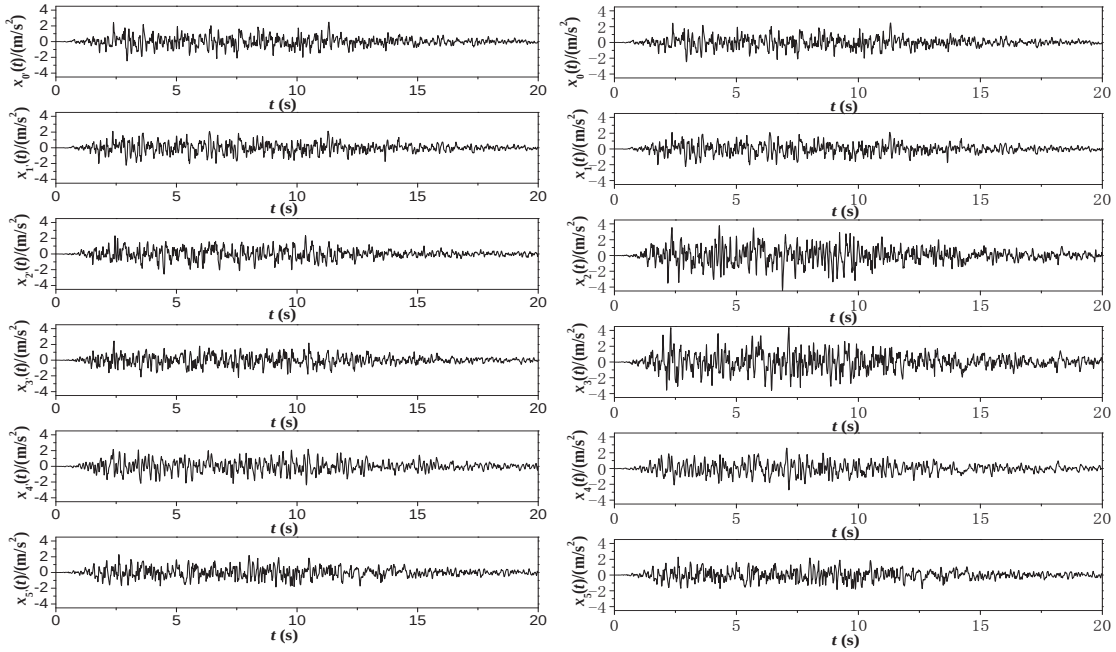

(a) On bedrock (b) On ground surface

Fig. 6 Simulated non-stationary ground motion acceleration time histories

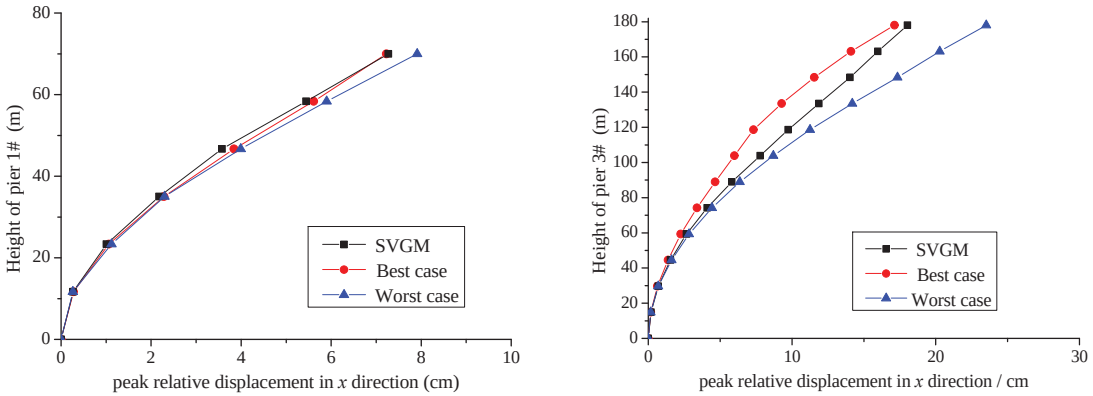

(a) Pier 1 (short) (b) Pier 3 (high)

Fig. 7 Peak relative displacements in transverse (x) direction up the pier height

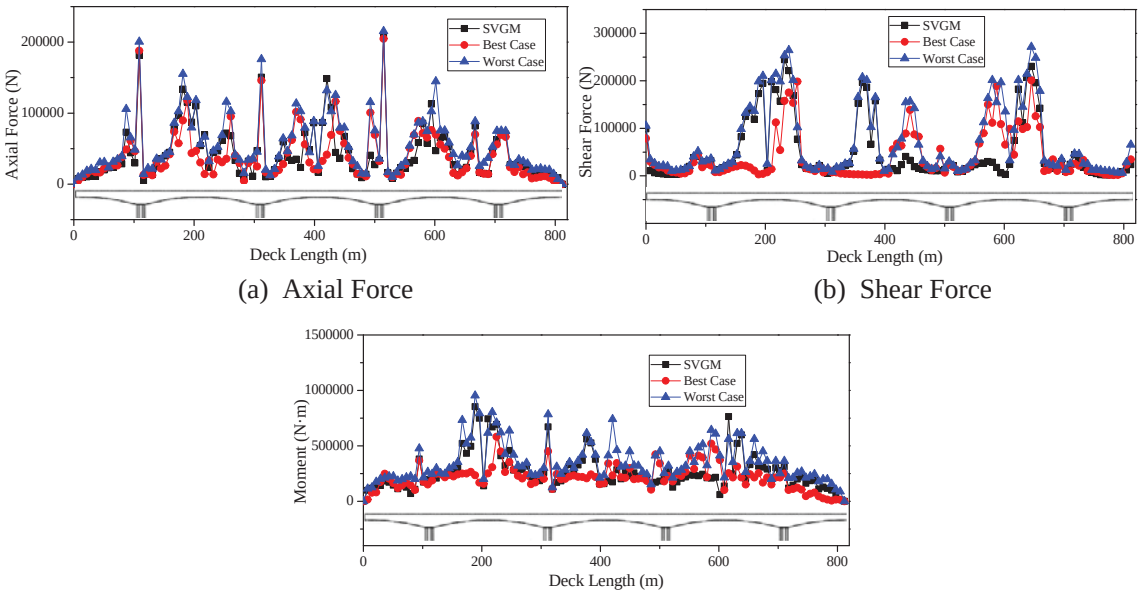

(a) Axial Force (b) Shear Force

(c) Moment

Fig. 8 Absolute internal force demand envelopes of the girder

(a) Compressive damage under the 'Best' case excitation

(b) Compressive damage under SVGM excitation

(c) Compressive damage under the 'Worst' case excitation

Fig. 9 Compressive damage for the three bedrock seismic excitation cases (in colour)

(a) Tensile damage under the 'Best' case excitation

(b) Tensile damage under SVGM excitation

(c) Tensile damage under the 'Worst' case excitation

Fig. 10 Tensile damage for the three bedrock seismic excitation cases (in colour)

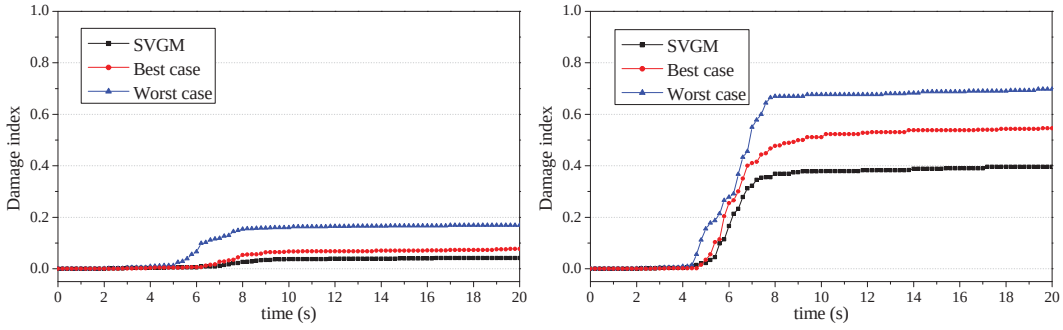

(a) Compressive damage (b) Tensile damage

Fig. 11 Damage development curves of the bottom tie beam on Pier 3

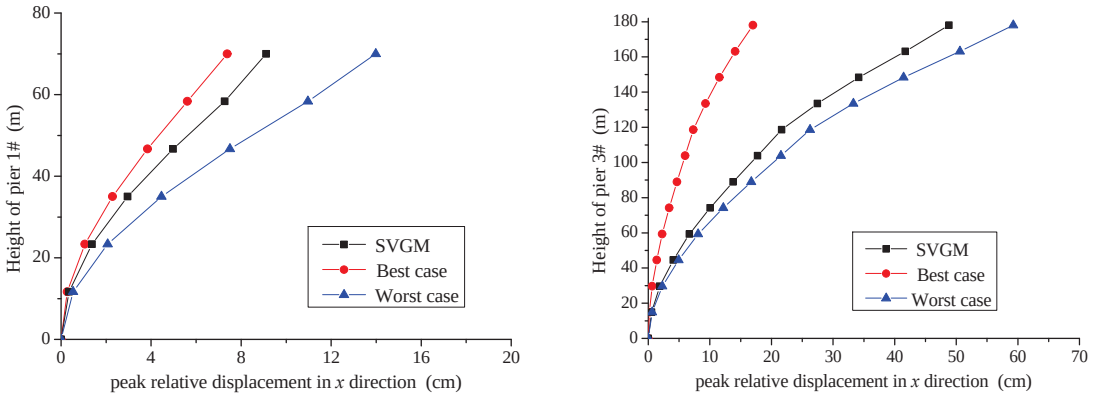

(a) Pier 1# (b) Pier 3#

Fig. 12 Peak relative displacements in transverse (x) direction up the pier height

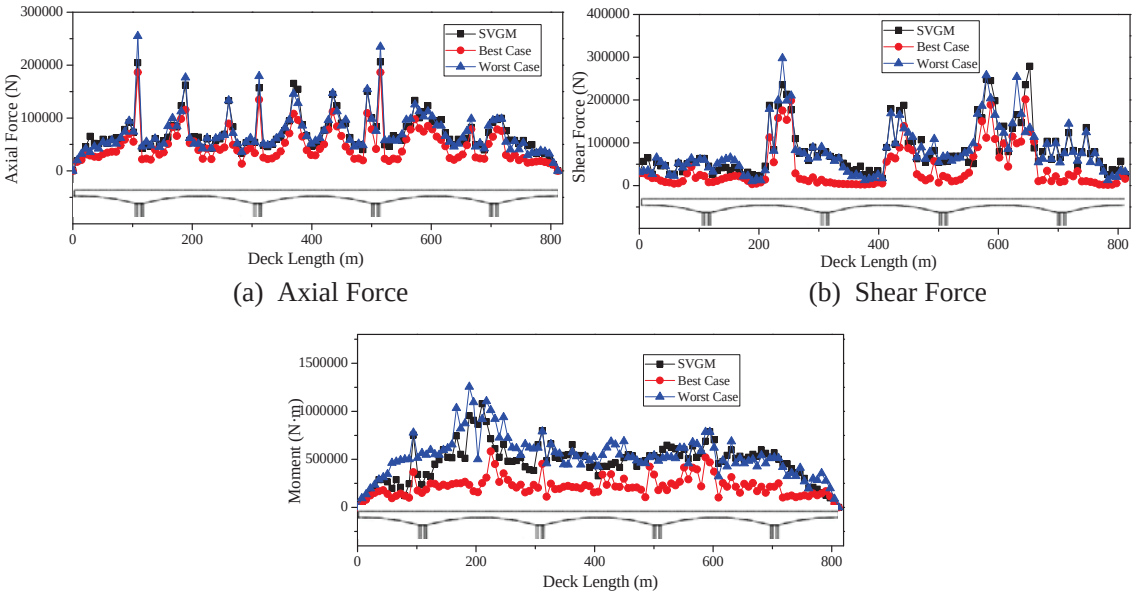

(a) Axial Force (b) Shear Force

(c) Moment

Fig. 13 Absolute internal force demand envelope of the girder

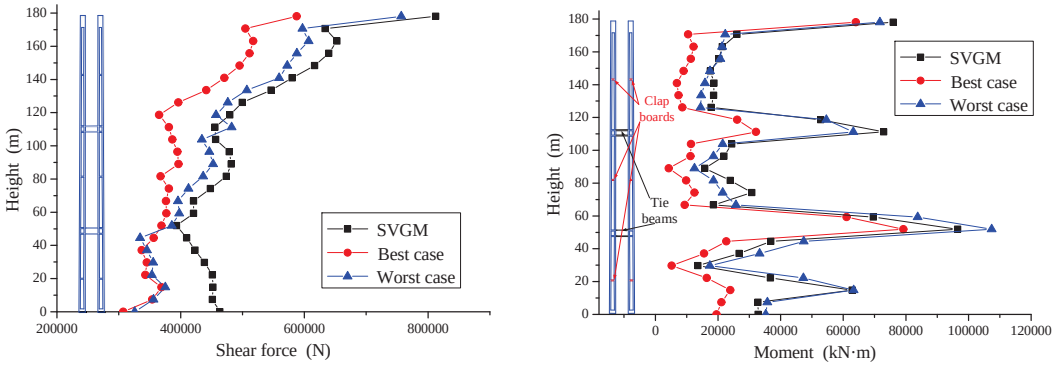

(a) Shear Force (b) Moment

Fig. 14 Absolute internal force demand envelope of Pier 2

(a) Compressive damage under the ‘Best’ case excitation

(b) Compressive damage under the SVGM excitation

(c) Compressive damage under the ‘Worst’ case excitation

Fig. 15 Compressive damage for the three ground surface seismic excitation cases (in colour)

(a) Tensile damage under the 'Best' case excitation

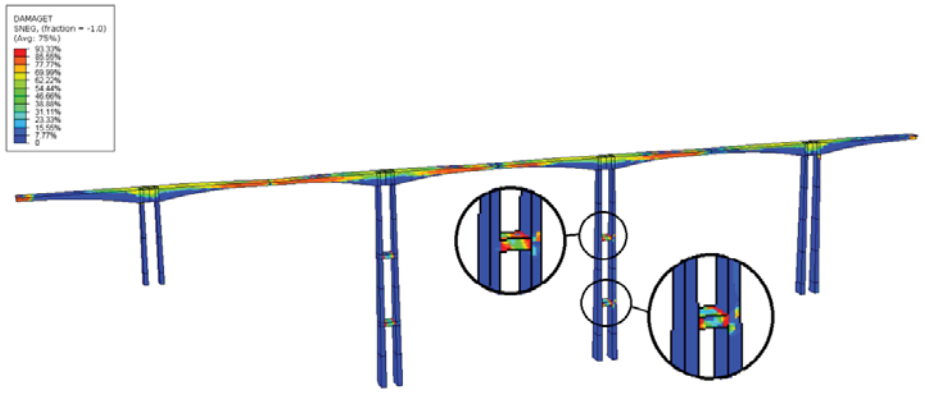

(b) Tensile damage under the SVGM excitation

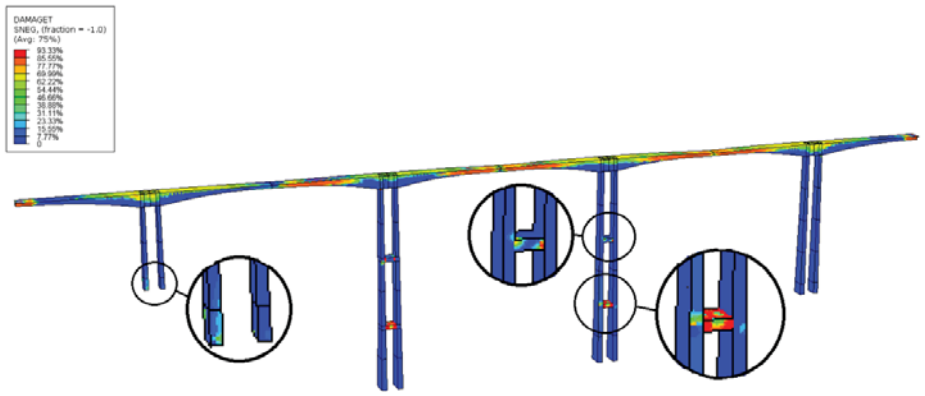

(c) Tensile damage under the 'Worst' case excitation

Fig. 16 Tensile damage for the three ground surface seismic excitation cases (in colour)

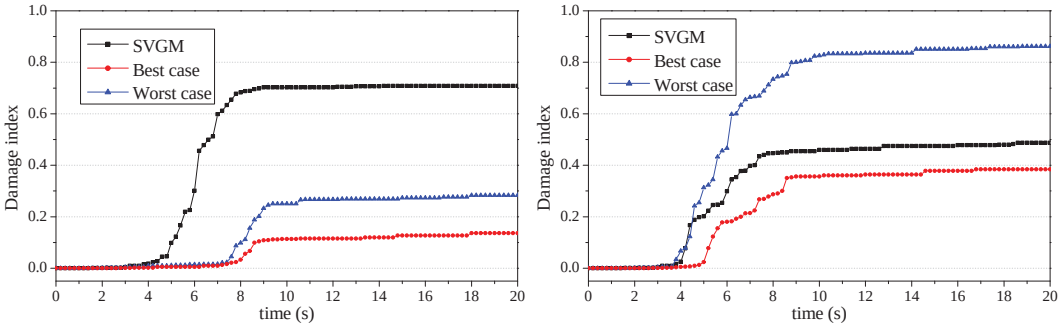

(a) Upper tie beam (b) Bottom tie beam

Fig. 17 Tensile damage development curves of the tie beams on Pier 3

Table 1 Dynamic parameters of concrete C50

Parameters of model	Value	Parameters of model	Value
Modulus of elasticity E (MPa)	36116	Ultimate compressive stress σ_{cu} (MPa)	42.92
Poisson's ratio v	0.2	Initial yield tensile stress σ_{t0} (MPa)	3.50
Density ρ (kg/m3)	2650	tensile recovery coefficient w_t	0
Dilation angle ψ (°)	30	Compressive recovery coefficient w_c	1
Initial yield compressive stress σ_{c0} (MPa)	19.47	Damping ratio ξ	0.05

Table 2 Characteristic parameters of the soil

Soil type	Density ρ (g•cm^{-3})	Shear wave velocity v (m/s)	Damping ratio ξ
Bedrock	2.8	1500	0.05
Strongly weathered shale	2.7	700	0.05
Pebble soil	2.1	500	0.1
Gravelly soil	1.8	400	0.1

Table 3 Excitation scenarios of ground motions

Excitation scenarios		Ground motion acceleration (transverse direction)
on bedrock (group 1)	1-SVGM	Non-uniform input as shown in Fig. 6(a)
	2-the 'Worst' case	Uniform input using $x_{2'}$ in Fig. 6(a)
	3-the 'Best' case	Uniform input using $x_{5'}$ in Fig. 6(a)
on ground surface (group 2)	4-SVGM	Non-uniform input as shown in Fig. 6(b)
	5-the 'Worst' case	Uniform input using x_2 in Fig. 6(b)
	6-the 'Best' case	Uniform input using x_5 in Fig. 6(b)

Table 4 Peak relative displacements at the top of piers under seismic excitations on bedrock

Pier number	transverse (x) direction (cm)			longitudinal (y) direction (cm)			vertical (z) direction (cm)		
	Best	SVGM	Worst	Best	SVGM	Worst	Best	SVGM	Worst
1	7.23	7.27	7.91	3.12	3.63	3.55	1.83	1.89	1.91
2	12.18	14.96	17.88	2.30	4.02	11.01	3.62	3.42	4.19
3	17.14	18.03	23.52	3.11	2.48	9.31	3.75	2.78	4.12
4	11.46	12.82	13.96	3.21	3.27	10.34	1.39	1.48	1.51

Table 5 Peak relative displacements at the top of piers under seismic excitations on ground surface

Pier number	transverse (x) direction (cm)			longitudinal (y) direction (cm)			vertical (z) direction (cm)		
	Best	SVGM	Worst	Best	SVGM	Worst	Best	SVGM	Worst
1	7.38	9.11	13.98	3.83	4.11	4.29	1.92	2.13	2.41
2	12.31	47.13	51.32	2.71	11.01	4.78	3.51	4.24	5.88
3	17.01	48.82	59.25	3.21	15.63	3.99	3.99	3.60	4.85
4	11.12	28.33	25.18	3.36	11.24	4.01	1.28	1.45	2.65